CHAPTER II

Characterization of mesophases: Experimental Techniques

CHAPTER II

Characterization of mesophases:

Experimental Techniques

Abstract

The experimental techniques used in this work for the detection and characterizations of the various mesophases are optical microscopy, differential scanning calorimetry and small angle X-ray diffraction methods. A brief discussion on the working principles of those methods along with their merits and limitations has been done in this chapter.

II. 1 Introduction

The importance of characterization of different mesophases arises from the dependence of the mechanical, electrical, magnetic and optical properties of mesogens on their various phases. The distinction between two mesophases is often very subtle due to the existence of large variety of liquid crystal phases. Identification and systematic classification of different mesophases have been done according to their distinct phase structures. Several techniques are used in conjunction with each other to identify the various mesophases. The most widely used technique of mesophase identification is optical microscopy, which reveals that each different mesophase has a distinct optical texture. The basic information in structure investigations is the description of the texture, the sum of the topological elements which are large enough to be observed under a polarizing microscope. Differential scanning calorimetry (DSC) is nearly always employed as a complimentary tool to the optical microscopy and reveals the mesophases by detecting the enthalpy change that is associated with a phase transition. However it cannot identify the type of mesophase, but the level of enthalpy change does give some information about the degree of molecular ordering within a mesophase. X-ray diffraction is the most powerful technique for the investigation of the microscopic structure of mesogens and hence for the indentification of the polymorphs. X-ray diffraction from the liquid crystal is just like Bragg scattering from crystals. It will map the positions of molecules within a phase and hence determine the phase structure and classification to which the particular phase belongs.

II. 2 Characterisation of Mesophases

II. 2. 1 *Optical polarization microscopy*

The most striking feature of liquid crystals is the wide variety of visual patterns they display under polarized light. These patterns called *textures* are due almost entirely to the defect structure that occurs in the long-range molecular order of the liquid crystals materials. For the determination of phase transition temperatures and the identification of liquid crystal phases, observation of textures is an important technique for the liquid crystal physicists. The identification of mesophases through optical polarizing microscopy usually involves the magnified view of a thin sample of a mesogenic material sandwiched (thickness ~ 10-20 μm) between a glass microscope slide and a glass cover slip. The microscope slide of material is placed in a hot stage, whose temperature is controlled usually between room temperature and 300°C, between polarizers, which are crossed at 90° to each other. With no sample and with isotropic sample the polarized light remains unaffected but with the anisotropic, birefringent sample an optical texture appears giving information relating to the arrangement of the molecules within the medium. The texture is found to depend on

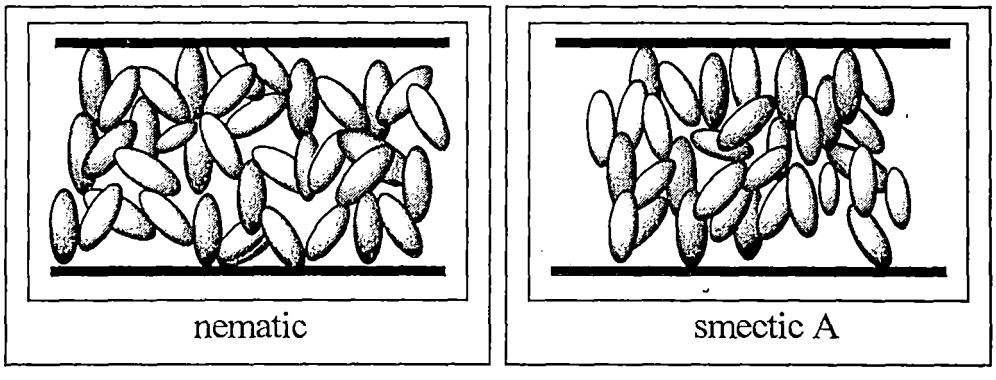

Figure II. 1 Homeotropic alignment of liquid crystals.

the alignment of the sample viz., whether homeotropic or homogeneous (planar) and the involved phase structure.

Homeotropic alignment is where the molecules that constitute the phase structure are oriented such that their long axes (optic axes) are normal to the supporting substrate (Fig.II.1). When the molecules are so oriented polarized light is unaffected by the material and so light cannot pass through the analyzer resulting in complete darkness to the observer.

In homogeneous (planar) alignment the constituent molecules of the liquid crystals phase are oriented parallel to the supporting substrates (Fig.II.2). With homogeneous alignment, a thin layer of the liquid crystals phase exhibits birefringence and a coloured texture results when viewed between crossed polarizers. Classification of different liquid crystalline phases by the observation of textures alone is often ambiguous, and other methods are needed to support it. Detailed description of various textures, with photographs, is given by Demus and Richter [1], Slaney et al. [2], Bouligand [3].

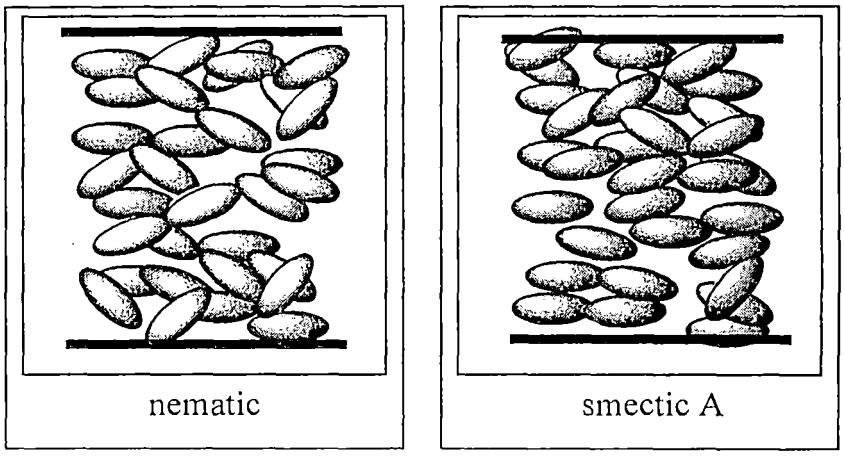

Figure II. 2 Homogeneous alignment of liquid crystals.

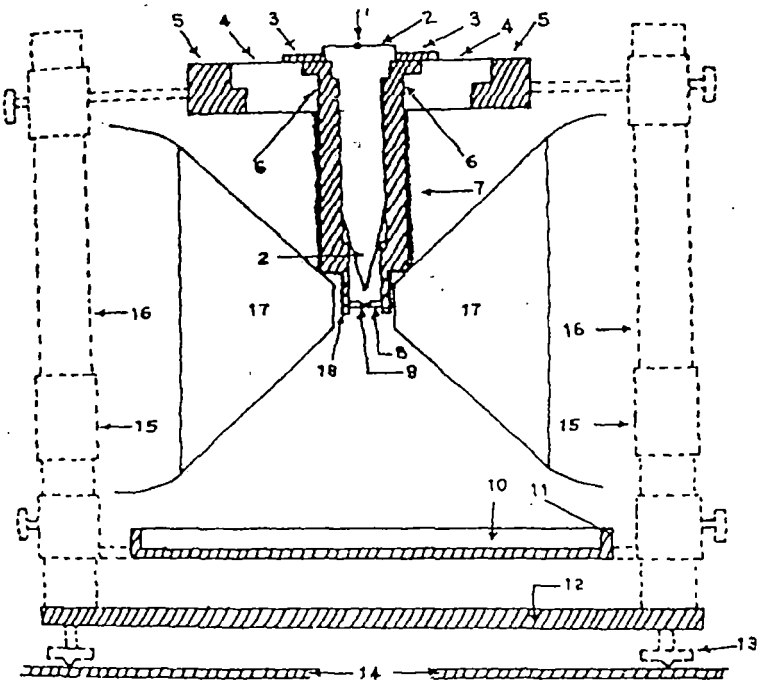

Figure II. 4 Schematic representation of the X-ray diffraction set up.

(1) Entrance of the X-ray beam, (2) Collimator, (3) Brass ring, (4) Ring of syndanyo board, (5) Brass ring, (6) Cylindrical Brass chamber, (7) Asbestors insulation and heater winding, (8) Specimen holder and thermocouple, (9) Sample position, (10) Film cassette, (11) Film cassette holder, (12) Base plate, (13) Leveling screw, (14) Brass plates over the coils of the electromagnet, (15) Removable spacer, (16) Supporting brass stand, (17) Pole pieces and (18) Asbestors.

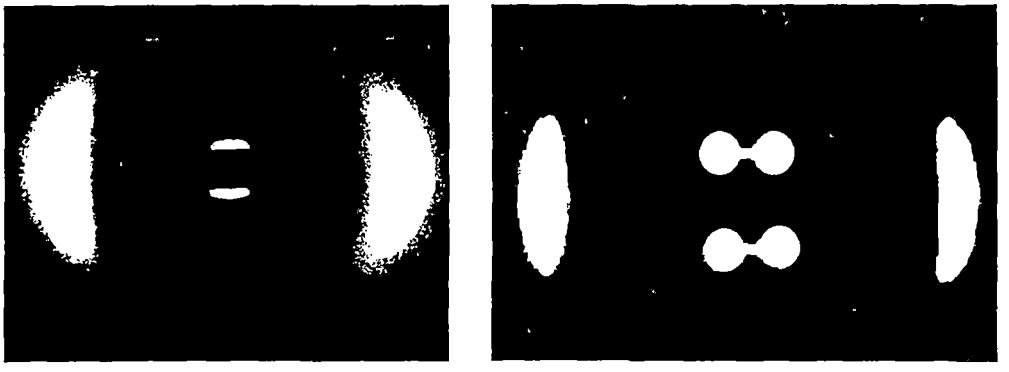

Ordinary Nematic phase Cybotactic Nematic phase

Figure II. 5 Typical diffraction photographs for nematic phase

II. 2. 2 *Differential scanning calorimetry*

Differential Scanning Calorimetry (DSC) reveals the presence of phase transitions in a material by detecting the enthalpy change associated with each phase transition. The level of enthalpy change provides some indication of the types of phase involved. Accordingly DSC was used in conjugation with Optical Polarization Microscopy to determine the type of mesophasees.

When a material melts, a change of state occurs from solid to liquid and this melting process requires energy (endothermic) from the surroundings. Converse is also true. The DSC instrument measures the energy absorbed or released by a sample as it is heated or cooled. Solid to liquid involves high energy of transition (enthalpy change around 30 to 40 kJmol-1). But more subtle structural phase changes involved in liquid crystals LC to LC and LC to isotropic liquid are reflected by relatively small enthalpy changes (1 to 2 kJmol-1). Mettler FP84 thermosystem or Pyris 6 DSC instrument was used for DSC studies. Typical DSC plots is shown in Fig.II.3.

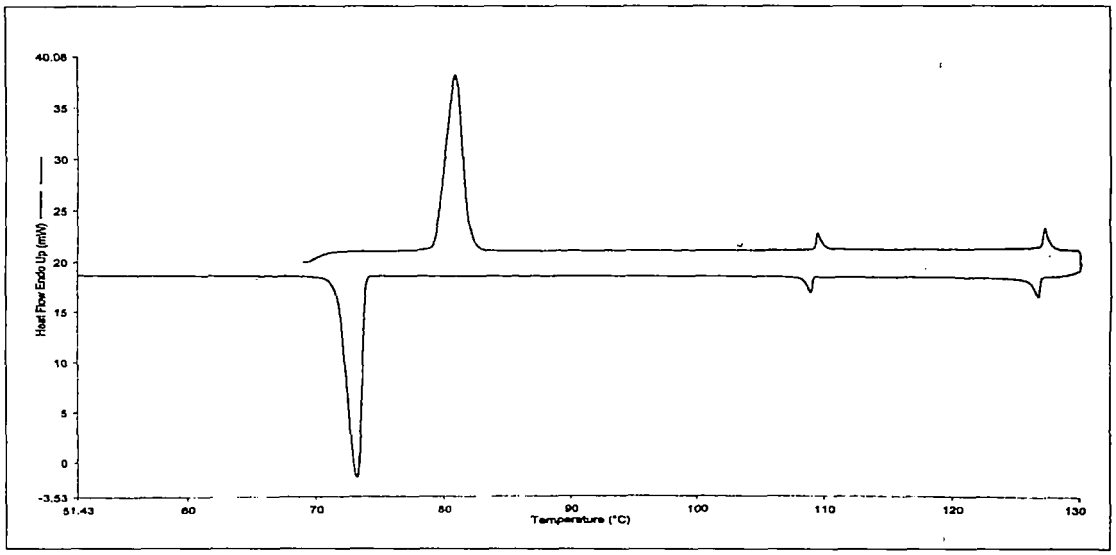

Figure II. 3 DSC plot of bis[4-(n-octyloxy)phenyl]diazene oxide.

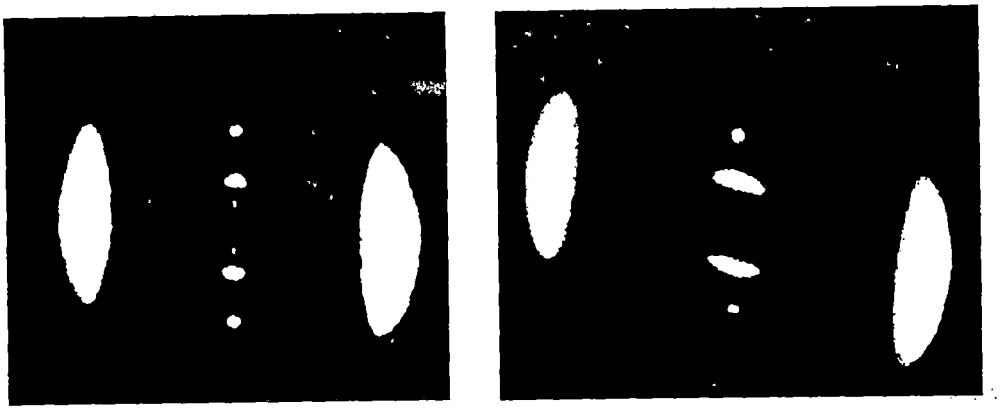

Smectic A phase Smectic C phase

Figure II. 6 Typical diffraction photographs for smectic phase.

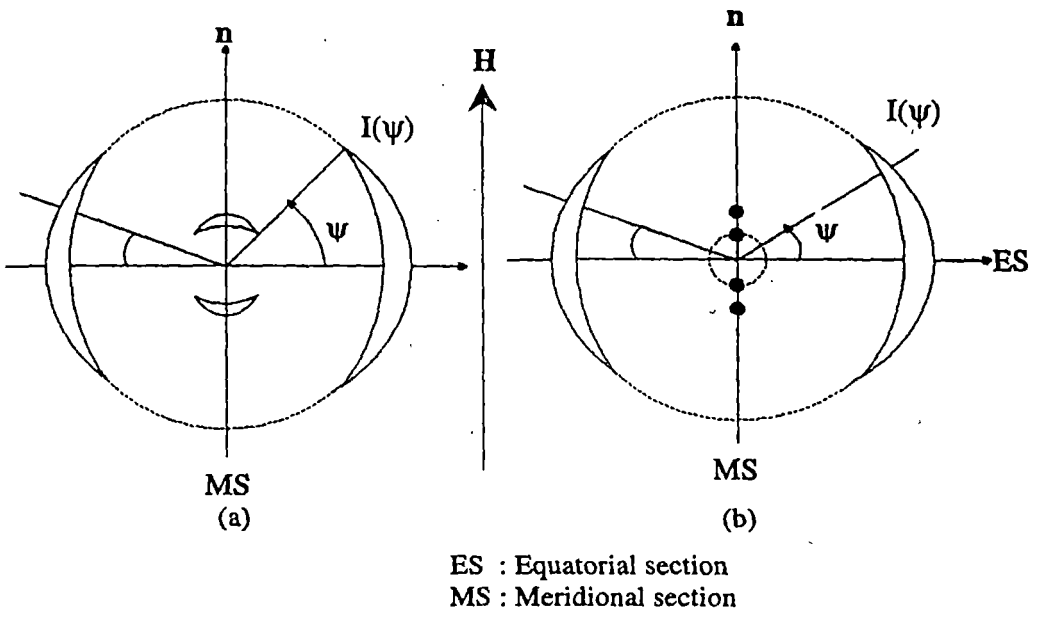

Figure II. 7 Schematic representation of the X-ray diffraction pattern of an oriented (a) nematic and (b) smectic A phase.

II. 2. 3 *Small angle X-ray diffraction*

Schematic diagram of the set-up used for X-ray diffraction studies is shown in Fig. II.4, which was fabricated earlier [4,5] at the Liquid Crystal Research Laboratory, Department of Physics, University of North Bengal. Small angle X-ray photographs were taken throughout the mesomorphic range using Nickel-filtered CuK_{α} radiation, the temperature was regulated within ±0.5°C by a controller, Indotherm 401-D2 (India). The sample was inserted by capillary action in a thin walled (~0.05mm) Lindemann glass capillary of 1mm diameter and was aligned by slow cooling from the isotropic phase to the desired temperature in presence of magnetic field of about 4-5 KG. All photographs were taken with X-rays perpendicular to the magnetic field direction.

Different types of diffraction patterns are obtained depending upon the type of the mesophases [5-14]. As a starting point for the discussion of the experimental results for X-ray scattering by nematic liquid crystals typical diffraction photographs of magnetically oriented samples are shown in Fig.II.5. The diffraction photographs for smectic phase are also given in Fig.II.6. The schematic representation of the X-ray diffraction pattern for nematic and smectic A phases are shown in Fig.II.7.

The diffraction pattern is neither that of the solid like crystal nor of isotropic liquid, but it looks like in between. Evidently two characteristic distances, parallel and perpendicular to **n** (or **H**) are present. However, unoriented nematic phase shows X-ray diffraction pattern which is a uniform halo just like that of an isotropic liquid. This is due to the fact that, generally a liquid crystal sample consists of a large number of domains, the molecules being aligned within each domain in a preferred direction,

i.e., the director, but there is no preferred direction for the sample as a whole and naturally, X-ray diffraction pattern has a symmetry of revolution around the direction of X-ray beam. The outer circular halo is split into two cresents having maxima along the equatorial direction ($\mathbf{n} \perp \mathbf{H}$), which are formed due to intermolecular scattering and the corresponding diffraction angle is a measure of average lateral intermolecular distance (D). These distances lie between 3.5 Å and 6.5 Å, lateral dimension of a typical mesogenic molecules and the average intermolecular distance are found to be around 5 Å.

For the situation $\mathbf{n} \parallel \mathbf{H}$, inner halo also has two crescents with maxima at much lower angle in the meridional direction. This diffraction peak must arise from correlations in the molecular arrangement along **n**. So by measuring the corresponding angles of diffraction one gets the value of the apparent molecular length (*l*).

For skewed cybotactic nematic phase, inner halo splits into four spots or appears as dumbbell shaped as shown in Fig.II.8. In the case of smectic phases, the inner pattern appears as sharp spots, sometimes second order spots are found. From these second order spots the translational order parameter τ can also be determined.

The apparent molecular length for nematic phase and layer thickness for smectic phase are calculated using Bragg equation, but the average intermolecular distance (D) are determined using a modified Bragg formula $D = 1.117\lambda/2\sin\theta$ derived by de Vries [18,19] on the arguments of cylindrical symmetry. The interplaner spacing (*l*) of cybotactic group [16, 20, 21] is calculated using Bragg relation and length of the building unit (L') is calculated using the relation $\beta_t = \cos^{-1}(l / L')$, where β_t is the tilt

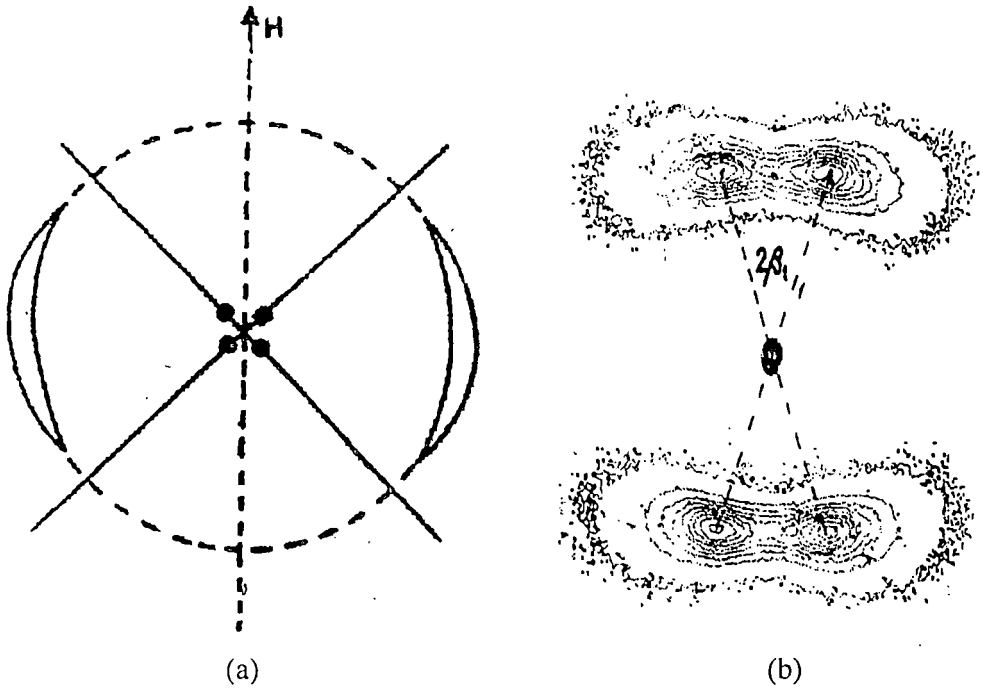

Figure II. 8 (a) Linear scanning directions for inner halo in cybotactic phase. (b) Intensity contour map of the inner hallo (broad view) of X-ray diffraction pattern of skewed cybotactic nematic phase showing tilt angle β_t.

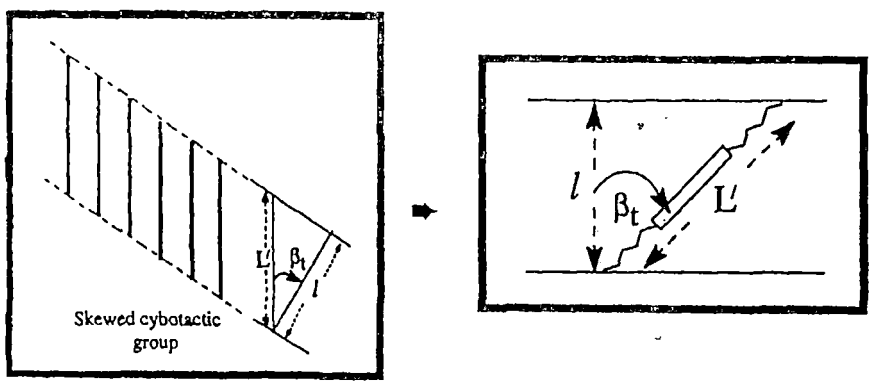

Figure II.9 Tilt angle β_t in the skewed cybotactic nematic phase.

angle (Figure II. 9) and is measured directly from photograph. When β_t cannot be measured from the film one calculates it using the above relation and assuming L = L', where L is the model length of the molecules. Orientational distribution function f(β) and orientational order parameters $< P_L >$ are calculated from the azimuthal intensity profile of equatorial arcs in the X-ray diffraction pattern, following a procedure described below.

For the above analysis the X-ray photographs are scanned linearly and circularly by an optical microdensiometer (Carl Zeiss Jena MD 100, Germany) equipped with auto chart drive facility. Full circular scanning of optical density (OD) is done at an interval of 5 degrees considering the maximum OD position at an angle $\psi = 0°$. These OD data are converted to intensity using a calibration curve and following the procedure of Klug and Alexander [15]. The experimental intensity values were then corrected for background intensity values arising due to the air scattering. Thus we get angular intensity distribution I(ψ) vs. angle (ψ) curve. The orientational distribution function f(β) was calculated from the intensity distribution I(ψ) using the following relation given by Leadbetter and Norris [16].

$$I(\psi) = C \int_{\beta=\psi}^{\pi/2} f(\beta) \sec^2 \psi [\tan^2 \beta - \tan^2 \psi]^{-1/2} \sin \beta d\beta \qquad \text{.....2.1}$$

As molecular distribution in the nematic phase is centrosymmetric, the distribution function and the intensity can be expanded as even cosine power series.

$$I(\psi) = \sum_{n=0}^{r} a_{2n} \cos^{2n} \psi \qquad \text{....2.2}$$

$$f(\beta) = \sum_{n=0}^{r} b_{2n} \cos^{2n} \beta \qquad \text{....2.3}$$

Both the series converge rapidly. Retaining eight terms in the truncated series, a least square fitting was made with the observed I(ψ) values to get the coefficients of 2.2.

These values of a_{2n} were then used to calculate the coefficients of b_{2n} using the relation

$$b_{2n} = a_{2n} \frac{(2n+2)!}{2^{2n}(n!)^2} \qquad \text{.....2.4}$$

Orientational order parameter ⟨P2⟩ and ⟨P4⟩ were then calculated using the following equation

$$\langle P_L \rangle = \frac{\int P_L(\cos\beta) f(\beta) d(\cos\beta)}{\int f(\beta) d(\cos\beta)} \qquad \text{.....2.5}$$

Necessary computer program for this purpose has been developed by the research group of Liquid Crystal Research Laboratory, Department of Physics, North Bengal University. The uncertainties in l, D and β_t values are ±0.01, ±0.01 and ±0.1 respectively and that in ⟨P2⟩ and ⟨P4⟩ values are estimated to be ±0.02.

To find the exact distance between the sample and X-ray film aluminium-powder photograph was taken. The Bragg angle θ′ corresponding to the (hkl) reflecting plane for aluminium is given by [17].

$$\sin\theta' = \frac{\lambda}{2a}\sqrt{h^2 + k^2 + l^2} \qquad \text{.....2.6}$$

where a is the lattice constant of aluminium. Thus calculating the values of Bragg angles from above equation and measuring the diameter (D) of the diffraction rings corresponding to (111) and (222) reflections the actual distance (H) between the sample and the film can be found from the relation

$$\tan 2\theta' = \frac{D}{2H} \qquad \text{.....2.7}$$

Bragg angle for the peaks corresponding to l D parameters were then calculated using the above relation.

References

1. D. Demus and L. Richter, *Textures of Liquid Crystals*, Verlag Chemie, NY (1978).
2. A. J. Slaney, K. Takatohi and J. W. Goodby in *The Optics of Thermotropic Liquid Crystals*. Ed. S. Elston and R. Sambles, Taylor & Francis, 1998.
3. Y. Bouligand in *Handbook of Liquid Crystals*. Vol. 1 (Fundamentals), Ed. D. Demus, J. Goodby, G. W. Gray, H.-W. Spiess and V. Vill, WILEY-VCH, Verlag GmbH, Weinheim, FRG 1998.
4. B. Jha and R. Paul, *Proc. Nucl. Phys. and Solid State Phys. Symp.*, India. **19C**, 491 (1976).
5. B. Jha, S. Paul, R. Paul and P. Mandal, *Phase Transitions*, **15**, 39 (1989).
6. S. Diele, P. Brand and H. Sackmann, *Mol. Cryst. Liq. Cryst.*, **16**, 105 (1972).
7. A. de Vries, *Pramana, Suppl.* No. **1**, 93 (1975).
8. A. de Vries, A. Ekachi and N. Sielberg, *J. de Phys.*, **40**, C3-147 (1979).
9. A. J. Leadbetter, J. Prost, J. P. Gaughan and M. A. Mazid, *J. de Physique.*, **40**, C3-185 (1979).
10. A. J. Leadbetter and P.G. Wrighton, *J. de Physique.*, **40**, C3-238 (1979).
11. V. M. Sethna, A. de Vries and N. Spielberg, *Molecules, Cryst. Liq. Cryst.*, **62**, 141 (1980).
12. L. V. Azaroff and C. A. Schuman, *Molecules Cryst. Liq. Cryst.*, **122**, 309 (1985).
13. A. de Vries, *Mol. Cryst. Liq. Cryst.*, **131**, 125 (1985).
14. P. Mandal, M. Mitra, S. Paul and R. Paul, *Liq. Cryst.*, **2**, 183 (1987).

15. H. P. Klug and L. E. Alexander, "*X-ray Diffraction Procedures*", Jhon Wiley and Sons, NY, p-114 and p-473 (1994)

16. A. J. Leadbetter and E. K. Norris, *Molecules Phys.*, **38**, 669 (1979).

17. C. Kittle, *Introduction to Solid State Physics*, Wiley Eastern, Chapter 2 (1976).

18. A. de Vries, *Mol. Cryst. Liq. Cryst.*, **10**, 219 (1970).

19. A. de Vries, *Mol. Cryst. Liq. Cryst.*, **11**, 261 (1970).

20. I. G. Chistyakov and W. M. Chaikowsky, *Mol. Cryst. Liq. Cryst.*, **7**, 269 (1969).

21. A. de Vries, *Mol. Cryst. Liq. Cryst.*, **10**, 31 (1970).